



ARTICLE

Phage-free production of artificial ssDNA with *Escherichia coli*

Karl L. Behler¹  | Maximilian N. Honemann^{2,3}  | Ana R. Silva-Santos² |
Hendrik Dietz^{2,3} | Dirk Weuster-Botz¹

¹Technical University of Munich, School of Engineering and Design, Biochemical Engineering, Garching, Munich, Germany

²Technical University of Munich, Department of Physics, Biomolecular Nano-Technology, Garching, Munich, Germany

³Technical University of Munich, Munich Institute of Biomedical Engineering, Garching, Munich, Germany

Correspondence

Dirk Weuster-Botz, Chair of Biochemical Engineering, School of Engineering and Design, Technical University of Munich, Garching, Munich 85748, Germany.
Email: dirk.weuster-botz@tum.de

Funding information

Portuguese Foundation for Science and Technology, Grant/Award Number: PD/BD/135138/2017; German Research Foundation (DFG), Grant/Award Numbers: DI 1500/4-1, WE 2715/15-1

Abstract

Artificial single-stranded DNA (ssDNA) with user-defined sequences and lengths up to the kilobase range is increasingly needed in mass quantities to realize the potential of emerging technologies such as genome editing and DNA origami. However, currently available biotechnological approaches for mass-producing ssDNA require dedicated, and thus costly, fermentation infrastructure, because of the risk of cross-contaminating manufacturer plants with self-replicating phages. Here we overcome this problem with an efficient, scalable, and cross-contamination-free method for the phage-free biotechnological production of artificial ssDNA with *Escherichia coli*. Our system utilizes a designed phagemid and an optimized helper plasmid. The phagemid encodes one gene of the M13 phage genome and a freely chosen custom target sequence, while the helper plasmid encodes the other genes of the M13 phage. The phagemid particles produced with this method are not capable of self-replication in the absence of the helper plasmid. This enables cross-contamination-free biotechnological production of ssDNA at any contract manufacturer. Furthermore, we optimized the process parameters to reduce by-products and increased the maximal product concentration up to 83 mg L⁻¹ of ssDNA in a stirred-tank bioreactor, thus realizing up to a 40-fold increase in maximal product concentration over previous scalable phage-free ssDNA production methods.

KEYWORDS

biotechnological production, DNA origami, phagemid, process safety, ssDNA

1 | INTRODUCTION

Single-stranded DNA (ssDNA) occurs in nature commonly only in viruses or in a transient state when double-stranded DNA (dsDNA) is replicated. Lately, ssDNA came into scientific focus as a useful biopolymer for various applications. For example, in CRISPR/Cas-based genomic editing, long ssDNA donor strands with a length of 0.5–2 kb lead to higher insertion efficiencies (Bai et al., 2020; Quadros et al., 2017). In nanotechnology, ssDNA is used as a building

material for DNA origami, which is a bottom-up method for the construction of two- and three-dimensional nanoparticles with user-defined shapes (Dietz et al., 2009; Douglas, Dietz, et al., 2009; Rothmund, 2006). DNA origami nanoparticles are already used in many scientific fields (Derr et al., 2012; Douglas et al., 2007; Jungmann et al., 2010; Langecker et al., 2012; Pfitzner et al., 2013; Shaw et al., 2014) and are currently being explored for applications such as drug delivery systems or as direct therapeutic agents for virus neutralization (Andersen et al., 2009; Douglas et al., 2012;

This is an open access article under the terms of the Creative Commons Attribution License, which permits use, distribution and reproduction in any medium, provided the original work is properly cited.

© 2022 The Authors. *Biotechnology and Bioengineering* published by Wiley Periodicals LLC.

Li et al., 2018; Sigl et al., 2021; Zhao et al., 2012). These and other future applications will ultimately require mass quantities of custom-sequence ssDNA.

Although ssDNA can be chemically synthesized or produced in vitro by enzymatic processes (Ducani et al., 2013; Kishi et al., 2017; Kosuri & Church, 2014; Lizardi et al., 1998; Notomi et al., 2000; Veneziano et al., 2018; Walker et al., 1992), these methods can be costly and may not be easily amenable to scale up. To satisfy the need for scalable mass production of custom sequence ssDNA, biotechnological processes have been developed (Engelhardt et al., 2019; Praetorius et al., 2017). Genetically engineered M13-phages are produced in a high cell density cultivation (HCDC) and their ssDNA-genome is isolated for further use. However, this approach has limitations with respect to the length of user-defined sequence that can be inserted (Kick et al., 2015). To overcome the limitations of the M13 genome itself, Zinder and Boeke (1982) developed a so-called phagemid, a phage-plasmid-hybrid. This phagemid consists of a plasmid backbone, the M13 origin of replication, and its packaging signal (PS), leaving ample space for inserts with user-defined sequence. The phagemid can be produced as ssDNA and packaged into M13 phage capsids as the phagemid is recognized by the cell and phage machinery but has more space for the user-defined sequence (Engelhardt et al., 2019; Nafisi et al., 2018). To add the phage machinery to the cells, a helper phage or a helper plasmid is needed. The helper phage is an M13 phage with an impaired M13-ori (leading to less phage ssDNA; Vieira & Messing, 1987) whereas the helper plasmid is a plasmid comprised of the M13 genes and a plasmid backbone but without any regulatory sequences of the M13 phage (Chasteen et al., 2006). However, common methods using the helper plasmid provide limited yields of ssDNA up to 2 mg per liter (Shepherd et al., 2019). With the use of helper phages, the cells produce phagemid particles that contain the desired ssDNA in addition to complete helper phages that contaminate the product (Praetorius et al., 2017). The presence of the self-replicating helper phages is undesirable because it precludes running the aforementioned biotechnological processes for making ssDNA by contract manufacturers. This is because of the risk of cross-contaminating subsequent processes, since phages may not be cleaned from the fermentation equipment with 100% certainty by standard cleaning (cleaning in place CIP) and sterilization (sterilization in place SIP) procedures (Branston et al., 2013).

To enable the scalable production of high amounts of ssDNA without the use of self-replicating particles, we developed a new method called “reverse infection.” Here, *Escherichia coli* cells are first transformed with a helper plasmid, thus becoming a production strain. This strain can then be cultivated in a scalable HCDC process in a controlled stirred-tank bioreactor. Upon reaching the proper cell density, the cells are infected with phagemid particles—phage capsids containing only the phagemid as ssDNA—in the same way M13 phages can infect a cell (Krom et al., 2015; Qi et al., 2012). After infection, cells produce and package high amounts of the desired phagemid ssDNA as phagemid particles, which are not self-replicating

by themselves. To make this reverse infection setup possible, we designed a suitable set of phagemid and helper plasmid, since, as already described in the literature, *E. coli* cells that carry a helper plasmid normally develop a resistance to infection (Boeke et al., 1982; Brödel et al., 2016).

2 | MATERIALS AND METHODS

2.1 | Bacterial strain and media

In this study, an *E. coli* JM109 (*recA1, endA1, gyrA96, thi, hsdR17, supE44, relA1, Δ(lac-proAB)*, [F', *traD36, proAB, lacI^qZΔM15*]; Yanisch-Perron et al., 1985) was used for all cultivations and molecular biology. The bacterial strain was stored in medium with 15% glycerol at -80°C . Cultivations were performed in minimal medium (Riesenberg et al., 1991) which was prepared as described before (Kick et al., 2015). Cultures for molecular biology were grown in lysogeny broth (LB-medium). Agar plates were also made from LB-medium adding 20 g L^{-1} Agar-Agar.

2.2 | M13 phage

The M13 phage used here for preliminary studies was M13mp18RFP. For this variant of M13mp18, a constitutive expression cassette for red fluorescent protein (RFP) was integrated into the multiple cloning site using standard methods. Full sequence maps in Supporting Information: Supplement.

2.3 | Single-gene plasmids

For the study of each M13 gene, the respective coding sequences (CDS) were cloned into the backbone of the pCoLA Duet plasmid using Gibson assembly (Gibson et al., 2009). Expression was placed under the control of the Lac promoter and induced by the addition of 100 mM IPTG. Full sequence maps in Supporting Information: Supplement.

2.4 | Helper plasmid and phagemid

For the construction of all helper plasmid variants, the genome of M13KO7 (New England Biolabs) was used. For the basic helper plasmid variant (pfhp24), the F1-ori with PS was removed. Sequences inserted into the optimized helper plasmid (pfhp30) were synthesized by Integrated DNA Technologies (IDT). The phagemid was constructed using the plasmid backbone of a pBlueScript (Stratagene). Other plasmid features were obtained from the iGEM parts library. Custom sequences were synthesized by IDT or Genewiz (GENEWIZ Germany GmbH). It has a total length of 4843 bp with inserted user-defined sequence of 1024 bp. As user-defined sequence, we used a

De Bruijn sequence of fifth order. Full sequence maps in Supporting Information: Supplement.

2.5 | Phagemid particle preproduction

To preproduce phagemid particles, chemically competent *E. coli* JM109 was double transformed with a helper plasmid and a phagemid at the same time. Cells were plated on complex medium (2xYT) agar plates containing the respective antibiotics for the selection of both plasmids. Colonies were then picked and grown overnight in preculture tubes in 5 ml of complex medium (2xYT) also containing both antibiotics and 1.2 g L^{-1} of $\text{MgSO}_4 \times 7\text{H}_2\text{O}$ at 37°C while shaking at 250 rpm. Precultures were completely passaged to 500 ml baffled shaking flasks (DURAN® Baffled Flask, DWK Life Sciences GmbH) containing 50 ml of fresh medium (2xYT + 1.2 g L^{-1} of $\text{MgSO}_4 \times 7\text{H}_2\text{O}$ + antibiotics). Shaking flask cultivations were kept at 37°C and 200 rpm in a shaking incubator (WIS-20 shaking incubator, Witeg) for at least 8 h. Then cultures were centrifuged for 20 min at 12,000 rcf and the supernatant containing the preproduced phagemid particles was kept and stored at 4°C .

2.6 | Cultivations

Shaking flask cultivations for the study of the effects of single M13 genes were performed in 500 ml unbaffled shaking flasks. The flasks were filled with 50 ml of mineral medium (Riesenberg et al., 1991; Riesenberg-medium RB) containing 5 g L^{-1} glucose including Chloramphenicol and inoculated with 1 ml cell suspension at $\text{OD}_{600} = 0.3$. Subsequently, incubation was performed up to $\text{OD}_{600} = 0.2$ (Genesys 10S UV-VIS, Thermo Fisher Scientific Inc.) at 37°C and 200 rpm in a shaking incubator (WIS-20 shaking incubator, Witeg). This was followed by induction with 100 mM isopropyl β -D-1-thiogalactopyranoside (IPTG) and further incubation. Upon reaching an OD_{600} of 0.4 after ~ 1 h, infection was initiated with the appropriate phages with a multiplicity of infection (MOI) above 1 transforming unit per colony-forming unit (tfu cfu⁻¹) and further incubated overnight. MOI was estimated from the molar concentration of ssDNA molecules (see Sections 2.7 and 2.8) isolated from the phages, where 1 ssDNA molecule = 1 phage. In the end, fluorescence was measured from 200 μl cell suspension in a 96-well plate with a photometer (Infinite M2000, Tecan), cell density was measured in a photometer as before, and ssDNA concentration was measured in a nano volume photometer (N120, Implen) after isolation from 2 ml supernatant (see Section 2.7).

Shaking flask cultivations at varying production temperatures were performed in 1000 ml baffled shaking flasks (DURAN® Baffled Flask, DWK Life Sciences GmbH). The flasks were filled with 50 ml of mineral medium (Riesenberg et al., 1991; RB) containing 5 g L^{-1} glucose including Kanamycin and inoculated with 1 ml cell suspension at $\text{OD}_{600} = 0.3$. Subsequently, incubation was performed to $\text{OD}_{600} = 1$ at 37°C and 200 rpm in a shaking incubator (WIS-20 shaking incubator,

Witeg). After reaching this OD, cultures were diluted with an additional 50 ml of mineral medium (same as before) and infected with phagemid particles with an MOI of approximately 100 tfu cfu⁻¹. Subsequently, the cultures were further incubated overnight. Afterward, ssDNA concentration was analyzed from 2 ml supernatant (see Sections 2.7 and 2.8).

Pre-cultures for HCDC were prepared from cryostocks in two stages. In the first stage, *E. coli* cells were incubated in 50 ml of mineral medium (Riesenberg et al., 1991; RB; 5 g L^{-1} glucose) with Kanamycin in 500 ml baffled shaking flasks (DURAN® Baffled Flask, DWK Life Sciences GmbH) overnight at 37°C and 200 rpm in a shaking incubator (WIS-20 shaking incubator, Witeg). In the second stage, two times 100 ml of mineral medium (same as before) was inoculated with 10 ml of the first stage each and incubated in 1000 ml baffled shaking flasks as in the first stage for 6 h. Cells were centrifuged for reactor inoculation and concentrated tenfold in fresh mineral medium (same as before).

Controlled fed-batch cultivation processes of *E. coli* were performed using a stirred tank bioreactor with a working volume of 2.5 L (KLF Advanced System 3.6 L, Bioengineering AG). Cultivation was performed at pH 6.7 as previously described with a batch phase of about 10 h and an initial glucose concentration of 25 g L^{-1} followed by exponential feeding with 750 g L^{-1} glucose and a growth rate of μ_{set} of 0.15 h^{-1} (Kick et al., 2015). After exponential feeding for 14 h, the feed rate was reduced linearly within 1.5 h to a volumetric flow rate of 25 mL h^{-1} . Here, the dissolved oxygen (DO) concentration was controlled to 30% air saturation. The cultivation temperature was initially set to 37°C for all cultivations and, depending on the cultivation process, changed to the production temperature set point of 4.5 h after initiation of the feeding. 30 min later, infection was executed with phagemid particles with an MOI of approximately 1 tfu cfu⁻¹.

2.7 | Isolation of ssDNA

Samples of 2 ml were centrifuged for 10 min at 13,000 rcf and the supernatant was frozen directly for later processing. Each sampling was done in triplicates. The frozen samples were processed by thawing and adding 300 μl of 240 g L^{-1} polyethylene glycol (PEG) 8000 and 180 g L^{-1} NaCl solution. After 30 min incubation, samples were centrifuged for 10 min at 13,000 rcf, pellets were resuspended in 200 μl Tris-EDTA (TE)-buffer (10 mM Tris, 1 mM EDTA, pH 8.0) and phagemid-particles were lysed by adding 400 μl lysis buffer P2 (Qiagen) and incubated for approximately 60 s. The solution was neutralized by adding 300 μl neutralization buffer P3 (Qiagen). After 15 min of incubation on ice, samples were centrifuged again for 10 min at 13,000 rcf. Supernatants were mixed with 99% Ethanol 1:1 and incubated for 30 min on ice. After another round of centrifugation for 10 min at 13,000 rcf, the pellets were incubated in 75% ethanol for 10 min. After centrifuging as before, the ssDNA pellets were solved in 50–200 μl TE-buffer depending on pellet size. The downstream process for obtaining ssDNA from the culture was

basically the same as for the 2 ml samples, using 2.5% (w/v) PEG 8000 and 3% (w/v) NaCl instead for precipitating phagemid particles and was performed as described before (Kick et al., 2015).

2.8 | Analytics

The growth of the host cells was measured indirectly using optical density at 600 nm (Genesys 10S UV-VIS, Thermo Fisher Scientific Inc.) or by the determination of cell dry weight concentrations in triplicates. ssDNA concentration was determined in the supernatants by UV-absorption at 260 nm using a nano volume photometer (N120, Implen). Here too samples were measured three times, giving a total of 9 technical replicates for ssDNA concentration per sampling. Molar concentrations were calculated from the respective extinction coefficients which were calculated from the ssDNA sequence ($4.613 \times 10^7 \text{ M}^{-1} \text{ cm}^{-1}$; Tataurov et al., 2008). The coefficient was used for the entire DNA isolated from the phagemids. Thus it cannot reflect the correct amount of impurities as their extinction coefficients may vary. To differentiate between impurities and products, agarose gels (see Section 2.9) were analyzed using the software Fiji (open source, fiji.sc). The fraction of product ssDNA to total DNA was estimated by applying the gel-analysis tool of Fiji.

The fit of the ssDNA formation trend in the bioreactor with a sigmoidal function was estimated using MATLAB (The MathWorks Inc.) using the curve-fitting toolbox. The given 95% confidence bounds are calculated as nonsimultaneous, functional bounds.

2.9 | Agarose gel electrophoresis

Agarose gel electrophoresis (AGEP) was performed in 2% agarose gels containing 0.5× Tris-Borat EDTA (TBE) buffer (10×TBE, Carl Roth) and 5.5mM MgCl. The working voltage was 90 V for 1–1.5 h. Gels containing folded Origami were stained with ethidium bromide and all other gels with MIDORI Green Advance (Nippon Genetics Europe GmbH). For ethidium bromide, two drops of 0.025% solution were added to 50 ml of agarose gel. For MIDORI Green Advance 10 µl were added to 50 ml of agarose gel. The gels were imaged using an Intas exposure chamber (INTAS Science Imaging Instruments GmbH) and a Canon EOS 70D (Canon Inc.) or a Typhoon 9500 FLA Laser scanner (GE Healthcare Bio-Sciences AB) and post-processed as a whole (Adobe Photoshop CC). If not stated differently, the ladder used is the 1 kb Plus DNA Ladder from NEB (New England Biolabs). About 1000 ng of ssDNA from each reactor sample were plotted per lane if that amount could be isolated from the respective sample. Else less, but the maximal possible amount was plotted.

2.10 | Folding of the DNA origami structure

To confirm the correct sequence identity and quality of the scaffold, a brick-shaped 42-helix bundle was folded. The brick-like object was

designed using caDNA v.02 (Douglas, Marblestone, et al., 2009). The full list of oligonucleotides (S13) and design diagram (S12) is in the Supporting Information: Supplement. Chemically synthesized oligonucleotides were ordered from IDT. To determine the optimal folding condition, an initial folding screen according to Wagenbauer et al. (2017) was performed. Folded structures were purified using PEG precipitation and analyzed with agarose gels and negative stain transmission electron microscopy (TEM).

2.11 | Imaging

TEM grids were prepared by incubation of 5 µl of the purified or unpurified samples on formvar-supported carbon-coated Cu400 grids (Electron Microscopy Sciences) for 30–40 s. Excess sample was then blotted away and the grids were fixed with an aqueous 2% uranyl formate solution for 30 s. After drying, the grids were imaged using a transmission electron microscope (FEI Tecnai 120, FEI), operated at 120 kV, and a magnification of 30,000, resulting in a final pixel size of 3.56 Å per pixel. Images were acquired using the SerialEM software (Mastrorarde, 2005) and analyzed in the Software Fiji (open source, fiji.sc). 2D classifications were prepared using Relion 3.0 (Scheres, 2012).

3 | RESULTS AND DISCUSSION

The efficient production of biomolecules in microorganisms relies on a separation of biomass and product formation. This separation allows the microorganisms to grow to high cell density without the metabolic burden of product formation. For M13 phages especially the positive effect of the decoupling has been shown (Kick, Behler, et al., 2017). Additionally, bacterial cells infected with M13 phages stop phage production after a while (Smeal et al., 2017). Therefore, it is important, that the cells are only infected when a high amount of biomass has been produced. The “reverse infection” method described in this paper separates the production of biomass and product, by first growing cells with a helper plasmid that contains most of the phage genes. After sufficient biomass production, the cells are then infected with phagemid particles, that provide the missing gene, regulatory sequences, and the user-defined DNA sequence and allow for product formation. To be able to construct helper plasmids and phagemids for reverse infection, the effects of individual M13 genes were investigated first.

3.1 | Design of helper plasmid and phagemid

To identify the effects of individual M13 genes on ssDNA production after M13 phage infection, one or two genes of the M13 phage were cloned into a plasmid, in which a lac promoter controlled the gene expression. *E. coli* cells transformed with the individual plasmids were grown in shake flasks and infected with M13 phages. The latter

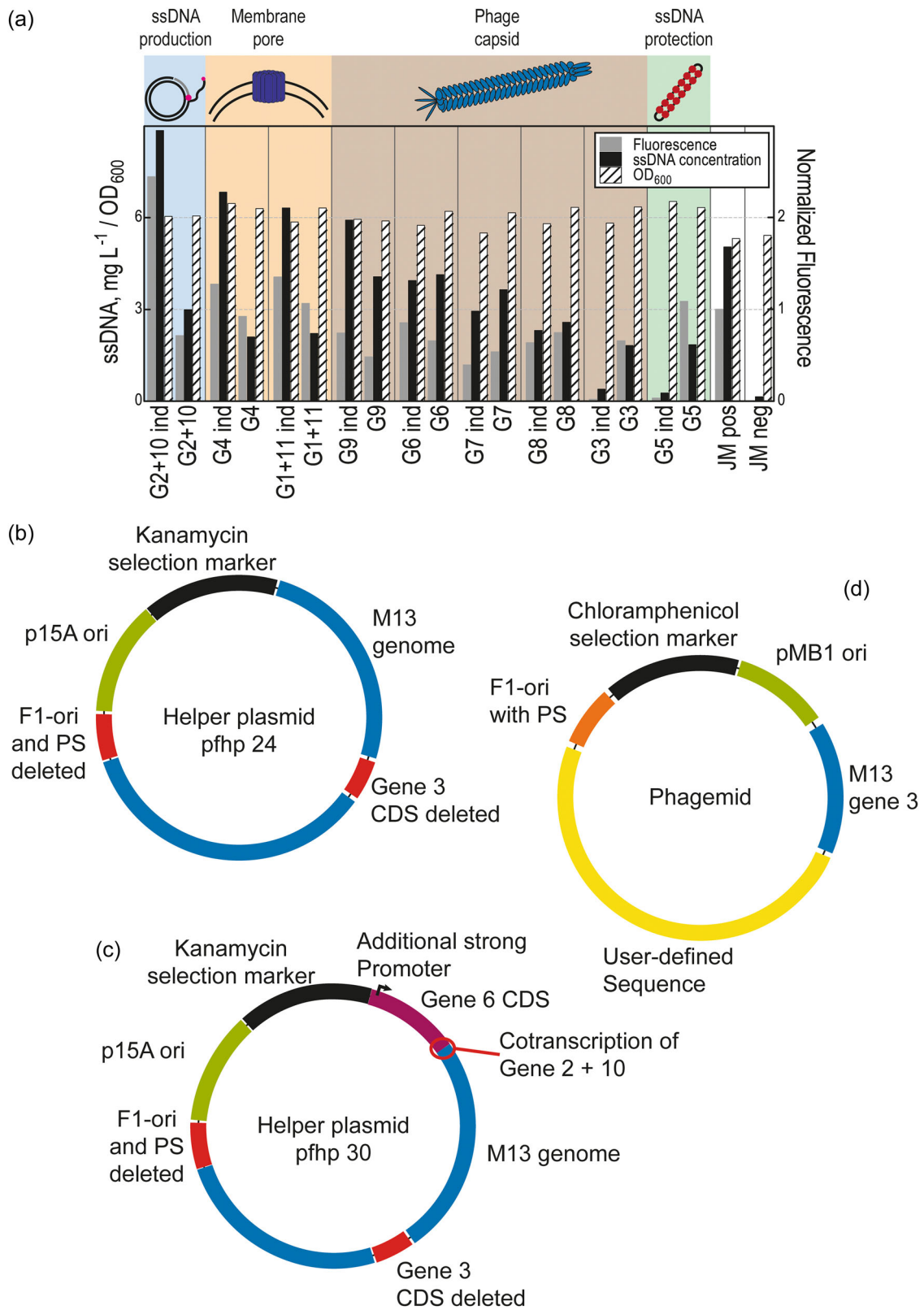


FIGURE 1 (See caption on next page)

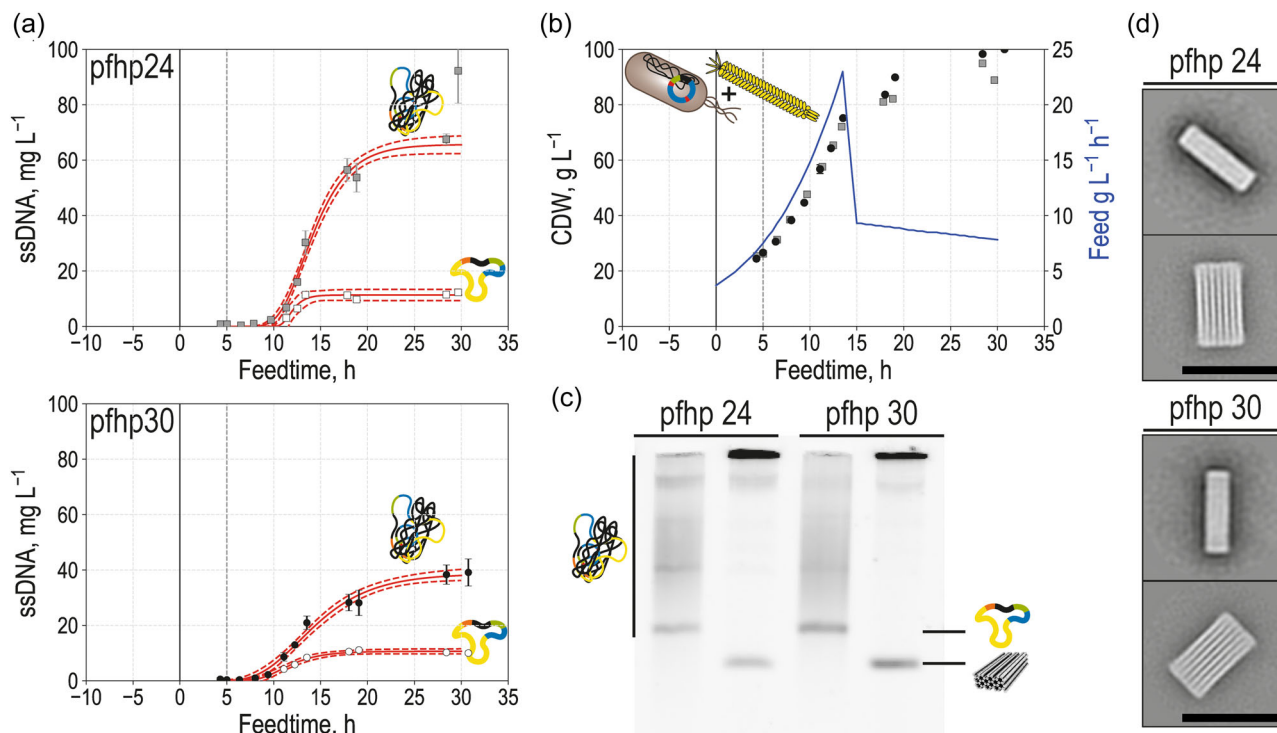


FIGURE 2 Two high cell density cultivations of *Escherichia coli* JM109 pfhp24 or pfhp30 in a 2.5-L stirred tank bioreactor at 37°C. Five hours after feed start, cells were infected with phagemid particles. (a) Variation of ssDNA concentration over feed time. Concentration was calculated from the measured absorbance at 260 nm (pfhp24: gray squares; pfhp30: black circles), then samples were analyzed by agarose gel electrophoresis (AGEP: S 1) to estimate the fraction of actual product ssDNA with Fiji (pfhp24: white squares; pfhp30: white circles). Error bars: standard deviation of technical replicates. Red lines: sigmoidal fit, solid; 95% confidence bounds, dashed. (b) Variation of cell dry weight (pfhp24: gray squares; pfhp30: black circles) and feed profile (Feed: volumetric glucose mass flow) over feed time. (c) AGEF of the ssDNA (scaffold) produced in this cultivation, as well as a 42-helix bundle folded with it. ssDNA taken at the end of the respective cultivation was not additionally purified before folding, and Origami-structures were not purified after folding. For pfhp24, the origami band accounts for 13% of the total lane intensity, while for pfhp30 it is 26% (Full AGEF: S 2). (d) Class-average micrographs of the folded 42-helix bundles. Scale bar: 50 nm (Fields of View: S 3, S 4).

additionally encoded an RFP as a marker for successful infection. The previously transferred genes were optionally induced by IPTG. No ssDNA production and no fluorescence were observed with the previously overexpressed gene 3 of the M13 phage (Figure 1a). The same effect was observed with overexpression of gene 5 before infection with the M13 phage. For cells overexpressing the additional genes 2 and 10, an increased ssDNA productivity could be observed. Individual overexpression of the other M13 genes did not cause any noteworthy effects (Figure 1a).

The increased productivity of the *E. coli* cells with prior overexpression of genes 2 and 10 may be explained by their function. The product of gene 2 (G2P) plays an important role in the replication of viral ssDNA and the product of gene 10 (G10P) protects the nascent ssDNA from hydrolysis (Mai-Prochnow et al., 2015). Thus, an increased amount of G2P and G10P in *E. coli* positively affects the amount of ssDNA formed by the cells after infection with M13 phages. The observation that overexpression of gene 5 before infection prevented phage production after the

FIGURE 1 Developing helper plasmid and phagemid. (a) Analysis of the infection resistance of *Escherichia coli* transformed with a plasmid coding for one or two genes of the M13 phage. Names of the bar-groups (e.g., G4 ind/G4) state the respective M13 gene transformed into these cells and whether expression was induced (ind) or not. JM pos is the positive control of JM 109 wild-type (WT) cells also infected with the respective M13 phage. (b) Schematic representation of the helper plasmid (phage free helper plasmid No. 24: pfhp 24) derived from helper phage M13KO7. Here, the coding sequence of gene 3 is deleted and the M13 origin of replication is replaced by the *rrnB1* terminator. Else all M13 genes are present in their natural order and regulation. (c) Schematic representation of the helper plasmid No. 30 (pfhp 30) based on pfhp 24. Here, a second gene 6 copy was placed downstream of an additional strong promoter directly upstream of the M13 genome. This will most likely result in co-transcription of genes 2 and 10 starting from the additional strong promoter. (d) The phagemid has a plasmid-ori (pMB1) to be propagated independently of the helper plasmid. Apart from the user-defined sequence, the phagemid contains the replication origin of the M13 phage including its packaging signal (PS) as well as the complete natural expression cassette of the M13 phage for its gene 3.

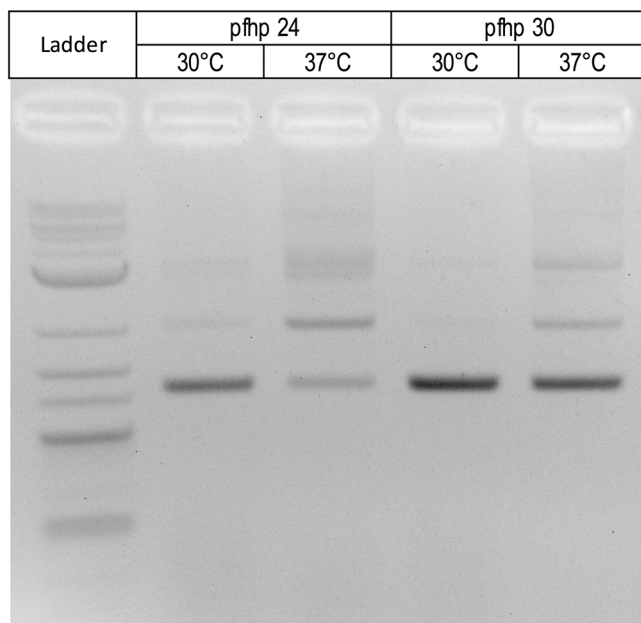


FIGURE 3 Agarose gel electrophoresis (AGEP) of ssDNA from four different shake flask (SK) cultivations. From left: Ladder; JM109 pfhp24 infected with the phagemid at 30°C; JM109 pfhp24 infected with the phagemid at 37°C; JM109 pfhp30 infected with the phagemid at 30°C; JM109 pfhp30 infected with the phagemid at 37°C. The leading band between 1200 and 1500 bp corresponds to the product. Bands above this correspond to by-products and contaminants.

infection has been shown recently, revealing that reduction of G5P levels can even increase the production of ssDNA with M13 phages (Lee et al., 2021). Since the product of gene 5 (G5P) binds to the phage ssDNA preventing conversion into dsDNA (Mai-Prochnow et al., 2015), strongly overexpressed G5P may completely prevent the formation of the replicative double-stranded form of the phage DNA. Natural levels of G5P however, should not exert an infection resistance. The resistance to M13 phage infection of the *E. coli* cells that occurs due to the prior overexpression of gene 3 has already been described in the literature (Boeke et al., 1982). The product of gene 3 (G3P) is one of the minor capsid proteins and is responsible for the infection of *E. coli* (Mai-Prochnow et al., 2015). How the product of gene 3 induces an infection resistance remains in the dark.

Based on these findings, a combination of helper plasmid and phagemid was first constructed that exploits the infection resistance caused by gene 3, as in this design variant our results fell in line with previous findings by Brödel et al. (2016, 2017). For this purpose, the coding sequence of gene 3 was first deleted from the helper plasmid (phage-free helper plasmid No. 24: pfhp 24, Figure 1b). Secondly, the expression cassette for gene 3 of the M13 phage was integrated into the sequence of the phagemid (Figure 1d). Thus, *E. coli* cells carrying the helper plasmid are not resistant to infection and the set of M13 genes is only completed upon infection so that new particles can be assembled. In our case, the phagemid additionally carries a substantial amount of user-defined sequence (random De Bruijn sequence of

fifth order) which can be used as a scaffold for DNA origami. We found with this design, that the removal of gene 5 from the helper plasmid was not necessary, as native expression of G5P does not cause an infection resistance.

An additional helper plasmid No. 30 (pfhp 30, Figure 1c) that overexpresses genes 2 and 10 was designed to account for the finding, that their overexpression increases the ssDNA yield. For this purpose, a strong constitutive promoter and a second copy of gene 6 were added upstream of genes 2 and 10. Thus co-transcribing genes 6, 2, and 10 with the strong promoter, should result in higher protein concentrations. The expression of gene 6 was increased, as this gene product is necessary for the proper termination of the phage capsid (Marvin, 1998; Rakonjac et al., 2011). Also, as shown before, higher expression levels of gene 6 did not cause any negative effects (Figure 1a).

3.2 | Phagemid production by high cell density cultivations

Phagemid (ssDNA) production with *E. coli* by combinations of helper plasmids (pfhp24 or pfhp30) and phagemid, as schematically shown in Figure 1b-d, was studied in controlled fed-batch processes in stirred tank bioreactors. For this purpose, the fed-batch process was performed in the same way as for ssDNA production with M13 phage infection (Kick et al., 2015). The *E. coli* cells carrying the helper plasmid were infected with phagemid particles 5 h after feeding was initiated. An MOI of approximately one phagemid particle per cell (tfu cfu^{-1}) was chosen for infection. Phagemid particles required for infection had been prepared in shake flasks by double transformation as previously described (Praetorius et al., 2017). As shown in Figure 2a, the ssDNA concentration in the medium of the stirred tank reactor increased approximately 5 h after infection and the maximum ssDNA concentration was measured after 30 h of feed time. A maximum concentration of 67 mg L^{-1} ssDNA was measured with *E. coli* cells carrying the helper plasmid pfhp24, whereas with the helper plasmid pfhp30 the final ssDNA concentration was 39 mg L^{-1} .

However, by analyzing the AGEPEP made of all samples throughout both cultivations, it becomes clear that in addition to the product band running at about 1300 bp, by-products and impurities are produced as well. Since the product concentration is determined by absorbance at 260 nm, these by-products distort the measured concentration. We determined the ratio of target ssDNA peak area intensity to total gel-lane intensity on the AGEPEP using the software Fiji. We estimated the amount of product ssDNA from the measured ratio of target ssDNA to total DNA. This gave us a similar amount for both reactor runs, with a maximum concentration of approx. 12 mg L^{-1} for pfhp24 and 11 mg L^{-1} for pfhp30. We also tested the thus produced scaffold DNA by running DNA origami folding reactions that produced the correct 42-helix bundle, however, the by-products caused a significant amount of aggregation.

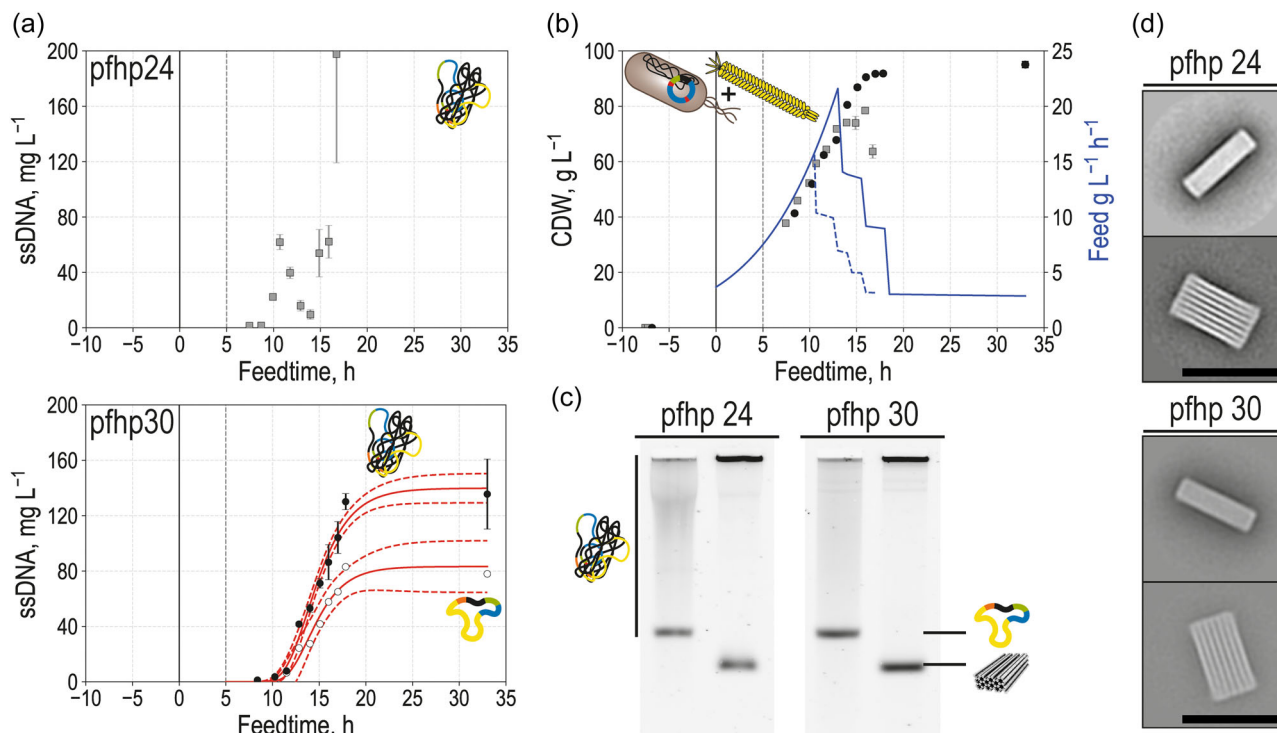


FIGURE 4 Two high cell density cultivations of *Escherichia coli* JM109 pfhp24 or *E. coli* JM109 pfhp30 in a 2.5-L stirred tank bioreactor at 30°C. Five hours after feed start, cells were infected with phagemid particles. (a) Variation of ssDNA concentration over feed time. Concentration was calculated from the measured absorbance at 260 nm (pfhp24: gray squares; pfhp30: black circles), then samples were analyzed by agarose gel electrophoresis (AGEP: S 6) to estimate the fraction of actual product ssDNA using Fiji (pfhp24: N/A; pfhp30: white circles). Error bars: standard deviation of technical replicates. Red lines: sigmoidal fit, solid; 95% confidence bounds, dashed. (b) Variation of cell dry weight (pfhp24: gray squares; pfhp30: black circles) and feed profile (pfhp24: dashed line; pfhp30: solid line) (Feed: volumetric glucose mass flow) over feed time. (c) AGEP of the ssDNA (scaffold) produced in this cultivation, as well as a 42-helix bundle folded with it. ssDNA taken at the end of the respective cultivation was not additionally purified before folding, and Origami-structures were not purified after folding. For pfhp24, the origami band accounts for 19% of the total lane intensity, while for pfhp30 it is 50% (Full AGEP: S 7). (d) Class-average micrographs of the folded 42-helix bundles. Scale bar: 50 nm (Fields of View: S 8, S 9).

For both helper plasmids, a similar amount of scaffold ssDNA could be obtained by HCDC. In both cases, the DNA origami used for quality control folded well. The helper plasmid pfhp30 produced a product with far fewer impurities and by-products. In comparison to double transformed cell approaches, at this point we already achieved around a fivefold increased maximal concentration of ssDNA (Chasteen et al., 2006; Shepherd et al., 2019). To further improve the production yield and to reduce the amount of impurities, whose elimination would require tedious downstream purification steps, we turned to optimize the process itself.

3.3 | Production process adaptations

As the effects of further alterations to the helper plasmids were hard to anticipate, the cultivation conditions were now investigated. Feed and infection were already optimized in previous studies (Kick et al., 2015; Kick, Hensler, et al., 2017). Therefore, only the temperature was considered as an influencing factor. Shake flask cultivations were performed at either 30°C or 37°C with both helper

plasmids. We found a significant decrease in by-product formation at 30°C (Figure 3). Additionally, product concentrations were on average more than three times higher. With cultivation at 30°C producing 3.25 mg L⁻¹ (pfhp24) and 4.15 mg L⁻¹ (pfhp30), cultivation at 37°C producing 1.07 mg L⁻¹ (pfhp24) and 1.36 mg L⁻¹ (pfhp30), respectively.

For pfhp30, production temperatures of 25°C and 34°C were also investigated (data not shown). When comparing all these shaking flask cultivations, 30°C was found to be optimal with respect to the combination of quality and quantity. Based on these results, HCDCs were also investigated at 30°C in the stirred tank bioreactor for both helper plasmids.

During cultivation with the helper plasmid pfhp24, a steep increase in the dynamic viscosity of the reactor medium was observed 10 h after the start of feeding, the cause of which is unknown (S 5). This meant that a sufficient oxygen supply could no longer be guaranteed. Thus the volumetric glucose mass flow had to be reduced to avoid oxygen limitation, as shown in Figure 4. For the same reason, the process had to be stopped after approximately 16 h. The product concentration over the course of cultivation shows no

clear trend, which in turn can also be attributed to the viscosity. With a high viscosity, product purification becomes very difficult, as cells cannot properly be separated from the medium by centrifugation.

As no clear trend in product concentration emerged in this cultivation, the amount of actual target scaffold ssDNA was not further analyzed, even though the amount of impurities visible in the AGEP of samples throughout the process appeared to be less than before (S 6).

For the production of ssDNA using the helper plasmid pfhp30 at 30°C, we also observed an increased viscosity in comparison to the 37°C run, albeit a lower increase than for pfhp24. Thus, even if the volumetric glucose mass flow also had to be reduced to still ensure sufficient oxygen supply, similarly high biomass concentrations were achieved as with the processes at 37°C. A maximum ssDNA concentration of about 135 mg_{ssDNA} L⁻¹ was achieved.

This process setup resulted in more ssDNA of a higher purity than before (Figure 4). No clear by-product bands are visible in the AGEP (S 6), leading to an estimated maximum concentration of

pure scaffold ssDNA of approximately 83 mg L⁻¹. The handling of the samples changes throughout the process due to the increase in viscosity. In the biotechnological process for high cell density production of M13-genome derived ssDNA, Kick, Behler, et al. (2017) show an optimal harvesting time after about 30 h of feeding. Here we recommend harvesting after 16–17 h of feeding as viscosity is still low enough for the downstream processing and production of ssDNA is almost at an end. A low batch-to-batch variance is also given until about 17 h after the start of feeding, as was shown in a second cultivation batch (S 10). The quality of the ssDNA was assessed by the folding of a DNA origami yielding a single sharp band in AGEP.

Thus, this process is suitable for the production of ssDNA with a high fraction of user-defined sequence with good purity and in large quantities. Concentrations of about 83 mg_{ssDNA} L⁻¹ are also comparable to the previously described process with helper phages (Praetorius et al., 2017). However, contamination of the target ssDNA with that of the helper phage is precluded by design, leading

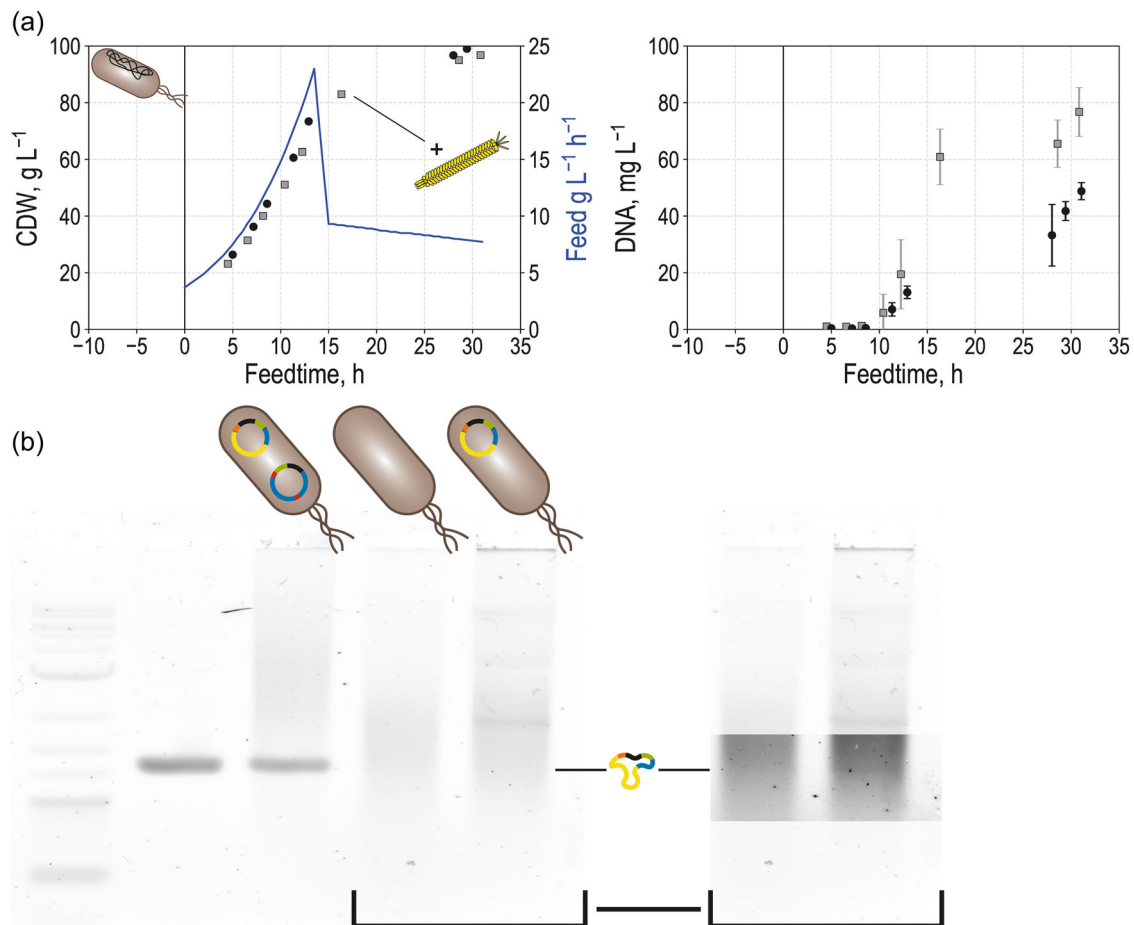


FIGURE 5 Two high cell density cultivations of *Escherichia coli* JM109 WT in a 2.5-L stirred tank bioreactor at 37°C. (a) Variation of cell dry weight, feed profile (Feed: volumetric glucose mass flow), and DNA concentration over feed time. In one cultivation cells were not infected at all (black circles) and in the other, strong contamination with phagemid particles was studied (gray squares). Error bars: standard deviation of technical replicates. (b) AGEP of the isolated DNA at the end of the cultivations. Lanes from left to right: Ladder; phagemid ssDNA reference; ssDNA from reverse infection production (pfhp30; 30°C); DNA prepped from cultivation without infection; DNA prepped from cultivation with contamination. To the right of the gel, the last two lanes of the gel are depicted again, with strongly increased contrast in the product ssDNA area (no bands are visible).

to an efficient and scalable new process for the production of ssDNA with user-defined sequences.

3.4 | Cross-contamination test with *E. coli*

Finally, to test that the phagemid particles produced in this way are not self-replicating and thus cannot cross-contaminate subsequent fermentation processes with *E. coli*, two cultivations with the *E. coli* JM109 wild type (without helper plasmid) were carried out at 37°C to represent standard cultivation conditions. One process served as a reference and the second simulated a strong contamination with phagemid particles.

In the reference process without phagemid infection, no discrete DNA species are formed as shown in the AGEF in Figure 5. The measured absolute DNA concentration in the supernatant increases slightly in a linear fashion after 10 h of feed time.

In a second process, to investigate process safety, contamination was simulated by injecting about 9.5×10^{10} phagemid particles in the stirred-tank reactor directly after inoculation, which corresponds to an MOI of about 0.24 tfu cfu⁻¹. In this high-cell density cultivation process, it could be shown that no phagemid ssDNA was formed over the entire process. The DNA visible in the AGEF was basically not different from the reference cultivation. Here, too, a linear increase can be seen when measuring the DNA concentration.

Crucially, it could be shown that the phagemid particles are not self-replicating and thus do not pose a danger for subsequent fermentation processes with *E. coli*. Compared to the reference cultivation, the infection directly after inoculation, shown in Figure 5, had little to no effect on this cultivation. This simulated contamination far exceeds the expected amount of phagemid particle residuals that should withstand incomplete reactor sterilization, as sterilization at 100°C for at least 20 min should already destroy all infective particles (Branston et al., 2013). Sterilizing a reactor at 120°C for at least 20 min, as usually done, leaves only a small chance for parts of the reactor to remain cooler than 100°C. (This in turn leaves only a very small chance for particles surviving sterilization much less 9.5×10^{10} particles.)

3.5 | Conclusion

The efficient and scalable production of artificial ssDNA with *E. coli* has been made possible with the “reverse infection” method. The phagemid particles used are not self-replicating even though they can infect *E. coli* cells. Large-scale production has been made feasible at any contract manufacturer as remaining, unwanted phagemid particles after cleaning and sterilization are of no consequence to other following production processes with *E. coli*. In the scalable fed-batch production process for artificial ssDNA, we achieved a 40-fold increase in maximal product concentration (83 mg L⁻¹ ssDNA), compared to the previous double transformation method (Shepherd et al., 2019), in a stirred tank bioreactor. The produced ssDNA was

free of contaminating DNA species that could interfere with downstream applications such as DNA origami folding.

AUTHOR CONTRIBUTIONS

Dirk Weuster-Botz and Hendrik Dietz designed the research. Karl L. Behler and Maximilian N. Honemann wrote the manuscript and designed the figures. Karl L. Behler designed and performed all cultivation experiments and designed all plasmids. Maximilian N. Honemann designed the DNA origami, contributed to the plasmid design, supervised the Origami folding, and performed all TEM imaging. Ana R. Silva-Santos performed the Origami folding and supported Karl L. Behler with plasmid cloning. All authors commented on the manuscript.

ACKNOWLEDGMENTS

The authors thank Ingmar Polte (Biochemical Engineering, TUM) for valuable discussions. Funding by the German Research Foundation (DFG) is gratefully acknowledged (grants WE 2715/15-1 and DI 1500/4-1). Ana R. Silva-Santos thanks the FCT—Portuguese Foundation for Science and Technology for PhD grant PD/BD/135138/2017 (BIOTECnico program). The support of Karl L. Behler by the TUM Graduate School (Technical University of Munich, Germany) is also acknowledged. Open Access funding enabled and organized by Projekt DEAL.

DATA AVAILABILITY STATEMENT

All data generated during this study are included in the submitted manuscript and its Supporting Information files. Raw data sets are available from the corresponding author on reasonable request.

ORCID

Karl L. Behler  <http://orcid.org/0000-0002-0969-5094>

Maximilian N. Honemann  <http://orcid.org/0000-0001-7805-906X>

REFERENCES

- Andersen, E. S., Dong, M., Nielsen, M. M., Jahn, K., Subramani, R., Mamdouh, W., Golas, M. M., Sander, B., Stark, H., Oliveira, C. L. P., Pedersen, J. S., Birkedal, V., Besenbacher, F., Gothelf, K. V., & Kjems, J. (2009). Self-assembly of a nanoscale DNA box with a controllable lid. *Nature*, 459(7243), 73–76. <https://doi.org/10.1038/nature07971>
- Bai, H., Liu, L., An, K., Lu, X., Harrison, M., Zhao, Y., Yan, R., Lu, Z., Li, S., Lin, S., Liang, F., & Qin, W. (2020). CRISPR/Cas9-mediated precise genome modification by a long ssDNA template in zebrafish. *BMC Genomics*, 21(1), 1–12. <https://doi.org/10.1186/s12864-020-6493-4>
- Boeke, J. D., Model, P., & Zinder, N. D. (1982). Effects of bacteriophage f1 gene III protein on the host cell membrane. *Molecular & General Genetics*, 16, 185–192.
- Branston, S. D., Stanley, E. C., Ward, J. M., & Keshavarz-Moore, E. (2013). Determination of the survival of bacteriophage M13 from chemical and physical challenges to assist in its sustainable bioprocessing. *Biotechnology and Bioprocess Engineering*, 18(3), 560–566. <https://doi.org/10.1007/s12257-012-0776-9>
- Brödel, A. K., Jaramillo, A., & Isalan, M. (2016). Engineering orthogonal dual transcription factors for multi-input synthetic promoters.

- Nature Communications*, 7, 13858. <https://doi.org/10.1038/ncomms13858>
- Brödel, A. K., Jaramillo, A., & Isalan, M. (2017). Intracellular directed evolution of proteins from combinatorial libraries based on conditional phage replication. *Nature Protocols*, 12(9), 1830–1843. <https://doi.org/10.1038/nprot.2017.084>
- Chasteen, L., Ayriss, J., Pavlik, P., & Bradbury, A. R. M. (2006). Eliminating helper phage from phage display. *Nucleic Acids Research*, 34(21), 1–11. <https://doi.org/10.1093/nar/gkl772>
- Derr, N. D., Goodman, B. S., Jungmann, R., Leschziner, A. E., Shih, W. M., & Reck-Peterson, S. L. (2012). Tug-of-war in motor protein ensembles revealed with a programmable DNA origami scaffold. *Science*, 338(6107), 662–665. <https://doi.org/10.1126/science.1226734>
- Dietz, H., Douglas, S. M., & Shih, W. M. (2009). Folding DNA into twisted and curved nanoscale shapes. *Science*, 325(5941), 725–730. <https://doi.org/10.1126/science.1174251>
- Douglas, S. M., Bachelet, I., & Church, G. M. (2012). A logic-gated nanorobot for targeted transport of molecular payloads. *Science*, 335(6070), 831–834. <https://doi.org/10.1126/science.1214081>
- Douglas, S. M., Chou, J. J., & Shih, W. M. (2007). DNA-nanotube-induced alignment of membrane proteins for NMR structure determination. *Proceedings of the National Academy of Sciences of the United States of America*, 104(16), 6644–6648. <https://doi.org/10.1073/pnas.0700930104>
- Douglas, S. M., Dietz, H., Liedl, T., Högberg, B., Graf, F., & Shih, W. M. (2009). Self-assembly of DNA into nanoscale three-dimensional shapes. *Nature*, 459, 414–418. <https://doi.org/10.1038/nature08016>
- Douglas, S. M., Marblestone, A. H., Teerapittayanon, S., Vazquez, A., Church, G. M., & Shih, W. M. (2009). Rapid prototyping of 3D DNA-origami shapes with caDNAno. *Nucleic Acids Research*, 37(15), 5001–5006. <https://doi.org/10.1093/nar/gkp436>
- Ducani, C., Kaul, C., Moche, M., Shih, W. M., & Högberg, B. (2013). Enzymatic production of “monoclonal stoichiometric” single-stranded DNA oligonucleotides. *Nature Methods*, 10(7), 647–652. <https://doi.org/10.1038/nmeth.2503>
- Engelhardt, F. A. S., Praetorius, F., Wachauf, C. H., Brüggenthies, G., Kohler, F., Kick, B., Kadletz, K. L., Pham, P. N., Behler, K. L., Gerling, T., & Dietz, H. (2019). Custom-size, functional, and durable DNA origami with design-specific scaffolds. *ACS Nano*, 13(5), 5015–5027. <https://doi.org/10.1021/acsnano.9b01025>
- Gibson, D. G., Young, L., Chuang, R.-Y., Venter, J. C., Hutchison, C. A., Smith, H. O., Iii, C. A. H., & America, N. (2009). Enzymatic assembly of DNA molecules up to several hundred kilobases. *Nature Methods*, 6(5), 343–345. <https://doi.org/10.1038/nmeth.1318>
- Jungmann, R., Steinhauer, C., Scheible, M., Kuzyk, A., Tinnefeld, P., & Simmel, F. C. (2010). Single-molecule kinetics and super-resolution microscopy by fluorescence imaging of transient binding on DNA origami. *Nano Letters*, 10(11), 4756–4761. <https://doi.org/10.1021/nl103427w>
- Kick, B., Behler, K. L., Severin, T. S., & Weuster-Botz, D. (2017). Chemostat studies of bacteriophage M13 infected *Escherichia coli* JM109 for continuous ssDNA production. *Journal of Biotechnology*, 258, 92–100. <https://doi.org/10.1016/j.jbiotec.2017.06.409>
- Kick, B., Hensler, S., Praetorius, F., Dietz, H., & Weuster-Botz, D. (2017). Specific growth rate and multiplicity of infection affect high-cell-density fermentation with bacteriophage M13 for ssDNA production. *Biotechnology and Bioengineering*, 114(4), 777–784. <https://doi.org/10.1002/bit.26200>
- Kick, B., Praetorius, F., Dietz, H., & Weuster-Botz, D. (2015). Efficient production of single-stranded phage DNA as scaffolds for DNA origami. *Nano Letters*, 15, 4672–4676. <https://doi.org/10.1021/acs.nanolett.5b01461>
- Kishi, J. Y., Schaus, T. E., Gopalkrishnan, N., Xuan, F., & Yin, P. (2017). Programmable autonomous synthesis of single-stranded DNA. *Nature Chemistry*, 10, 155–164. <https://doi.org/10.1038/nchem.2872>
- Kosuri, S., & Church, G. M. (2014). Large-scale de novo DNA synthesis: Technologies and applications. *Nature Methods*, 11(5), 499–507. <https://doi.org/10.1038/nmeth.2918>
- Krom, R. J., Bhargava, P., Lobritz, M. A., & Collins, J. J. (2015). Engineered phagemids for nonlytic, targeted antibacterial therapies. *Nano Letters*, 15(7), 4808–4813. <https://doi.org/10.1021/acs.nanolett.5b01943>
- Langecker, M., Arnaut, V., Martin, T. G., List, J., Renner, S., Mayer, M., Dietz, H., & Simmel, F. C. (2012). Synthetic lipid membrane channels formed by designed DNA nanostructures. *Science*, 338(6109), 932–936. <https://doi.org/10.1126/science.1225624>
- Lee, B., Lee, J., Ahn, D. J., Lee, S., & Oh, M. (2021). Optimizing protein V untranslated region sequence in M13 phage for increased production of single-stranded DNA for origami. *Nucleic Acids Research*, 49(11), 6596–6603.
- Li, S., Jiang, Q., Liu, S., Zhang, Y., Tian, Y., Song, C., Wang, J., Zou, Y., Anderson, G. J., Han, J. Y., Chang, Y., Liu, Y., Zhang, C., Chen, L., Zhou, G., Nie, G., Yan, H., Ding, B., & Zhao, Y. (2018). A DNA nanorobot functions as a cancer therapeutic in response to a molecular trigger in vivo. *Nature Biotechnology*, 36(3), 258–264. <https://doi.org/10.1038/nbt.4071>
- Lizardi, P. M., Huang, X., Zhu, Z., Bray-Ward, P., Thomas, D. C., & Ward, D. C. (1998). Mutation detection and single-molecule counting using isothermal rolling-circle amplification. *Nature Genetics*, 19(3), 225–232. <https://doi.org/10.1038/898>
- Mai-Prochnow, a, Hui, J. G. K., Kjelleberg, S., Rakonjac, J., McDougald, D., & Rice, S. A. (2015). Big things in small packages: The genetics of filamentous phage and effects on fitness of their host. *FEMS Microbiology Reviews*, 39(4), 465–487. <https://doi.org/10.1093/femsre/fuu007>
- Marvin, D. (1998). Filamentous phage structure, infection and assembly. *Current Opinion in Structural Biology*, 8(2), 150–158. [https://doi.org/10.1016/S0959-440X\(98\)80032-8](https://doi.org/10.1016/S0959-440X(98)80032-8)
- Mastronarde, D. N. (2005). Automated electron microscope tomography using robust prediction of specimen movements. *Journal of Structural Biology*, 152(1), 36–51. <https://doi.org/10.1016/j.jsb.2005.07.007>
- Nafisi, P. M., Aksel, T., & Douglas, S. M. (2018). Construction of a novel phagemid to produce custom DNA origami scaffolds. *Synthetic Biology*, 3(1), 1–8. <https://doi.org/10.1093/synbio/ysy015>
- Notomi, T., Okayama, H., Masubuchi, H., Yonekawa, T., Watanabe, K., Amino, N., & Hase, T. (2000). Loop-mediated isothermal amplification of DNA. *Nucleic Acids Research*, 28(12):e63.
- Pfützner, E., Wachauf, C., Kilchherr, F., Pelz, B., Shih, W. M., Rief, M., & Dietz, H. (2013). Rigid DNA beams for high-resolution single-molecule mechanics. *Angewandte Chemie-International Edition*, 52(30), 7766–7771. <https://doi.org/10.1002/anie.201302727>
- Praetorius, F., Kick, B., Behler, K. L., Honemann, M. N., Weuster-Botz, D., & Dietz, H. (2017). Biotechnological mass production of DNA origami. *Nature*, 552(7683), 84–87. <https://doi.org/10.1038/nature24650>
- Qi, H., Lu, H., Qiu, H.-J., Petrenko, V., & Liu, A. (2012). Phagemid vectors for phage display: Properties, characteristics and construction. *Journal of Molecular Biology*, 417(3), 129–143. <https://doi.org/10.1016/j.jmb.2012.01.038>
- Quadros, R. M., Miura, H., Harms, D. W., Akatsuka, H., Sato, T., Aida, T., Redder, R., Richardson, G. P., Inagaki, Y., Sakai, D., Buckley, S. M., Seshacharyulu, P., Batra, S. K., Behlke, M. A., Zeiner, S. A., Jacubi, A. M., Izu, Y., Thoreson, W. B., Urness, L. D., ... Gurumurthy, C. B. (2017). Easi-CRISPR: A robust method for one-step generation of mice carrying conditional and insertion alleles using long ssDNA donors and CRISPR ribonucleoproteins. *Genome Biology*, 18(1), 1–15. <https://doi.org/10.1186/s13059-017-1220-4>

- Rakonjac, J., Bennett, N. J., Spagnuolo, J., Gagic, D., & Russel, M. (2011). Filamentous bacteriophage: Biology, phage display and nanotechnology applications. *Current Issues in Molecular Biology*, 13(2), 51–76. <https://doi.org/10.1002/9780470015902.a0000777>
- Riesenberg, D., Schulz, V., Knorre, W. A., Pohl, H. D., Korz, D., Sanders, E. A., Ross, A., & Deckwer, W. D. (1991). High cell density cultivation of *Escherichia coli* at controlled specific growth rate. *Journal of Biotechnology*, 20(1), 17–27. <http://www.ncbi.nlm.nih.gov/pubmed/1367313>
- Rothemund, P. W. K. (2006). Folding DNA to create nanoscale shapes and patterns. *Nature*, 440(7082), 297–302. <https://doi.org/10.1038/nature04586>
- Scheres, S. H. W. (2012). RELION: Implementation of a Bayesian approach to cryo-EM structure determination. *Journal of Structural Biology*, 180(3), 519–530. <https://doi.org/10.1016/j.jsb.2012.09.006>
- Shaw, A., Lundin, V., Petrova, E., Fördos, F., Benson, E., Al-Amin, A., Herland, A., Blokzijl, A., Högberg, B., & Teixeira, A. I. (2014). Spatial control of membrane receptor function using ligand nanocalipers. *Nature Methods*, 11(8), 841–846. <https://doi.org/10.1038/nmeth.3025>
- Shepherd, T. R., Du, R. R., Huang, H., Wamhoff, E. C., & Bathe, M. (2019). Bioproduction of pure, kilobase-scale single-stranded DNA. *Scientific Reports*, 9(1), 1–9. <https://doi.org/10.1038/s41598-019-42665-1>
- Sigl, C., Willner, E. M., Engelen, W., Kretzmann, J. A., Sachenbacher, K., Liedl, A., Kolbe, F., Wilsch, F., Aghvami, S. A., Protzer, U., Hagan, M. F., Fraden, S., & Dietz, H. (2021). Programmable icosahedral shell system for virus trapping. *Nature Materials*, 20, 1281–1289. <https://doi.org/10.1038/s41563-021-01020-4>
- Smeal, S. W., Schmitt, M. A., Rodrigues, R., Prasad, A., & Fisk, J. D. (2017). Simulation of the M13 life cycle II: Investigation of the control mechanisms of M13 infection and establishment of the carrier state. *Virology*, 500, 275–284. <https://doi.org/10.1016/j.virol.2016.08.015>
- Tataurov, A. V., You, Y., & Owczarzy, R. (2008). Predicting ultraviolet spectrum of single stranded and double stranded deoxyribonucleic acids. *Biophysical Chemistry*, 133(1–3), 66–70. <https://doi.org/10.1016/j.bpc.2007.12.004>
- Veneziano, R., Shepherd, T. R., Ratanalert, S., Bellou, L., Tao, C., & Bathe, M. (2018). In vitro synthesis of gene-length single-stranded DNA. *Scientific Reports*, 8(1), 1–7. <https://doi.org/10.1038/s41598-018-24677-5>
- Vieira, J., & Messing, J. (1987). Production of single-stranded plasmid DNA. *Methods in Enzymology*, 153(1982), 3–11. [https://doi.org/10.1016/0076-6879\(87\)53044-0](https://doi.org/10.1016/0076-6879(87)53044-0)
- Wagenbauer, K. F., Engelhardt, F. A. S., Stahl, E., Hechtel, V. K., Stömmer, P., Seebacher, F., Meregalli, L., Ketterer, P., Gerling, T., & Dietz, H. (2017). How we make DNA origami. *ChemBioChem*, 18(19), 1873–1885. <https://doi.org/10.1002/cbic.201700377>
- Walker, G. T., Fraiser, M. S., Schram, J. L., Little, M. C., Nadeau, J. G., & Malinowski, D. P. (1992). Strand displacement amplification – An isothermal, in vitro DNA amplification technique. *Nucleic Acids Research*, 20(7), 1691–1696. <https://doi.org/10.1093/nar/20.7.1691>
- Yanisch-Perron, C., Vieira, J., & Messing, J. (1985). Improved M13 phage cloning vectors and host strains: Nucleotide sequences of the M13mp18 and pUC19 vectors. *Gene*, 33(1), 103–119. [https://doi.org/10.1016/0378-1119\(85\)90120-9](https://doi.org/10.1016/0378-1119(85)90120-9)
- Zhao, Y. X., Shaw, A., Zeng, X., Benson, E., Nyström, A. M., & Högberg, B. (2012). DNA origami delivery system for cancer therapy with tunable release properties. *ACS Nano*, 6(10), 8684–8691. <https://doi.org/10.1021/nn3022662>
- Zinder, N. D., & Boeke, J. D. (1982). The filamentous phage (Ff) as vectors for recombinant DNA—A review. *Gene*, 19(1), 1–10. [https://doi.org/10.1016/0378-1119\(82\)90183-4](https://doi.org/10.1016/0378-1119(82)90183-4)

SUPPORTING INFORMATION

Additional supporting information can be found online in the Supporting Information section at the end of this article.

How to cite this article: Behler, K. L., Honemann, M. N., Silva-Santos, A. R., Dietz, H., & Weuster-Botz, D. (2022). Phage-free production of artificial ssDNA with *Escherichia coli*. *Biotechnology and Bioengineering*, 119, 2878–2889. <https://doi.org/10.1002/bit.28171>